JCTC Journal of Chemical Theory and Computation

Article

pubs.acs.org/JCTC

Efficient Quantum Simulations of Metals within the Γ-Point Approximation: Application to Carbon and Inorganic 1D and 2D Materials

Mahdi Ghorbani-Asl,[†,‡] Rosalba Juarez-Mosqueda,[†] Agnieszka Kuc,[†] and Thomas Heine*[,†]

[†]School of Engineering and Science, Jacobs University Bremen, 28759 Bremen, Germany

[‡]Institut für Theoretische Festkörperphysik, Karlsruher Institüt für Technologie (KIT), Wolfgang Gaede Strasse 1, 76131 Karlsruhe, Germany

Supporting Information

ABSTRACT: Molecular dynamics simulations using quantum mechanics for the electronic system, i.e., within the Born−Oppenheimer or related Car−Parrinello approximation, became feasible and popular in recent years for very large systems. The most common setup for these simulations is the supercell method in conjunction with the Γ-point approximation. Here we provide a tool which is useful to choose the supercell of the considered system such that it makes it appear to have either an as large as possible band gap (optimized for Car−Parrinello setup) or the metallic character reflected at the Γ point (e.g., fold the Dirac point to the Γ point for graphene and carbon nanotubes) in order to monitor the metallic character in a trajectory. We address carbon nanotubes, graphene, and inorganic TS_2 analogues with T = Re, Nb. We further provide a simple Hückel code, which allows checking the electronic states close to the Fermi level within the Γ-point approximation, and we test its predictions against the density-functional-based tight-binding approach.

INTRODUCTION

Simulation of the processes and properties of extended nanostructures such as cabon nanotubes,[1] graphene,[2] and inorganic materials[3−11] or large biological molecules[12,13] using quantum-mechanical approaches to describe the electronic system has become feasible over recent decades due to tremendous progress in the development of computer hardware, parallel computing, numerical algorithms, quantum-mechanical methodology, and modern software implementations. Advantages of quantum-mechanical approaches over classical approaches for simulation of large nanostructures are their straightforward application without the need to parametrize or validate a force field, high transferability (application of the same approach to different material classes which allows comparative studies as well as describing interfaces), often also higher accuracy of structural parameters, energies, and mechanical properties, and, very importantly, access to the electronic system that allows simulation of chemical reactions and evaluation of properties using quantum-mechanical expectation values. The density-functional-based tight-binding (DFTB) method[14−16] was a pioneering approach to extend quantum-mechanical simulations to the nanoscale.[17,18] Already in the late 1990s it was shown that properties of nanostructured materials can be simulated using the DFTB method in appreciable quality, most notably STM images,[19] electronic conductivity,[20,21] or in special cases even NMR chemical shifts.[22]

Computational investigation of nanostructures implies that systems of several 1000 to some 100 000 electrons and more need to be treated. Besides DFTB, various other quantum-mechanical approaches have been used in this context, including semiempirical methods[23] and density-functional theory in different flavors of implementation, such as using pseudopotentials and plane waves,[24] the projected augmented wave method,[25] or local basis functions.[26]

A stationary quantum-mechanical system is typically a boundary condition problem. This means that correct description of the system boundaries is essential if a calculation shall give realistic results. As system sizes of 100−10 000 atoms are typically still too small to describe a typical complete nanoscopic system and as the boundaries of the nanoparticles are in most cases unknown from experiment, it is a very convenient and realistic approach to use the supercell technique. Here, spurious boundary effects are avoided by repeating the model structure in the three directions of space, i.e., by applying periodic boundary conditions. If the supercell is large, the reciprocal cell is small, and it is commonly accepted that the Γ-point approximation, i.e., choosing exactly one k point with $k = 0$ in the Brillouin zone, is valid. The Γ-point approximation has the advantage that the complex part of the Bloch functions collapses to real numbers, which greatly simplifies any software implementation and improves significantly the computational performance in terms of numerical operations and memory consumption.

It has been known for a long time that, in particular, for systems containing high symmetry the Γ-point approximation may not reflect the correct electronic density of states. As illustrated later, if a metallic carbon nanotube is modeled and the Dirac point is not folded onto the Γ point, the metallic character of the structure is not observed in the electronic levels available from this calculation. This may happen even for very

Received: May 3, 2012

 © XXXX American Chemical Society dx.doi.org/10.1021/ct3003496 | J. Chem. Theory Comput. XXXX, XXX, XXX−XXX

large supercells and could be misinterpreted if quantum-mechanical methods are used in a black box manner. Moreover, for more complex systems it may not be obvious to predict if the chosen simulation box indeed gives the correct information about the electronic structure of the system.

In this article, we propose to use simple Hückel or empirical orthogonal tight-binding theory to precalculate the electronic structure of supercells as validation for the choice of structural model, which will be used afterward for simulation employing a higher level method. In Hückel theory, only one orbital per atom is considered and expected to participate in the electronic subsystem that characterizes the material as metallic, that is, the states close to the Fermi level are dominated by those orbitals.[27] Hence, few inexpensive calculations reveal relevant information of the system that allows making a much better choice of the simulation box. For example, if the Car–Parrinello method shall be employed for the target system, it may be wise to use a supercell where the energy level differences between the conduction and the valence band at the Γ point are maximized, while for simulations using the Born–Oppenheimer technique it might be a better choice to use a simulation box where the metallic character of the system is reflected in the Γ point. This may be particularly useful for nanoelectromechanical simulations (electronic properties as a function of the system strain) or if the influence of dopants or defects shall be investigated. Moreover, the Hückel calculations may be useful for gaining a better understanding of the electronic structure of the system.

We have chosen carbon and inorganic 1D and 2D nanostructures, which are of strong interest in current research, as benchmark systems (Figure 1). While the results shown here

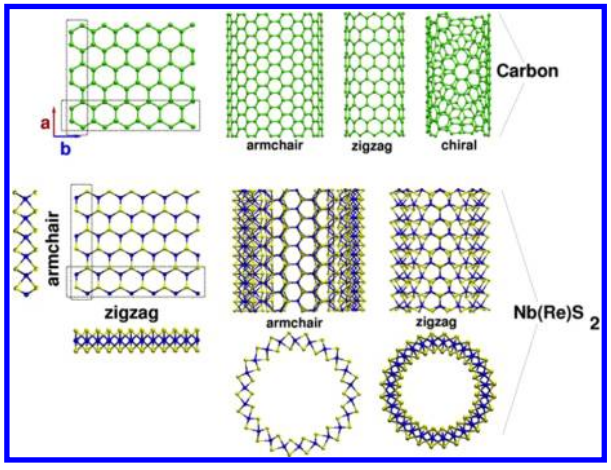

Figure 1. Sample structures of the 2D and 1D forms of carbon (graphene and carbon nanotubes) and corresponding inorganic TS_2 (T = Nb, Re) materials. Arrows show the direction of the lattice vectors for the layered structures. Dashed rectangles indicate the units in zigzag and armchair directions.

have been expected for many of the discussed carbon-based systems, we also show that this strategy is even useful for estimation of the electronic properties close to the Fermi level of transition-metal dichalcogenide nanostructures.

We developed a code that allows periodic Hückel calculations and a parameter table that allows Hückel band structure calculations within the DFTB+ program.[28] The code and parameter table are available as Supporting Information.

In this article, we show that the description of the electronic structure close to the Fermi level may fail for metallic systems. We rationalize this problem for a series of metallic carbon nanotubes of chiralities (n,m) with $(n - m)/3 \in I$, graphene, and graphene nanoribbons and show that only selected supercell sizes can give realistic numbers for the electronic structure, in particular, of the band gap, close to the Fermi level.

METHODS

It is well known that the Hückel method is a simple albeit powerful tool to include the qualitative structure of the quantum-mechanical π system for aromatic and sp^2-based carbon systems, including nanotubes and fullerenes.[29,30] We have written a basic Hückel theory program with periodic boundary conditions within the Γ-point approximation. The off-diagonal elements of the Hückel matrix are either zero (no bonds) or one (covalent bond). Bonds are determined through a distance criterion, and for bonds crossing the box boundaries the minimum image convention is applied. For carbon sytems, interatomic distances smaller than 1.5 Å define a bond ($H_{ij} = 1$) and for all other elements $H_{ij} = 0$, implying a reference energy of the noninteracting orbitals to be 0. After diagonalization of H_{ij}, the eigenvalues give the electronic energy levels in units of β, for which we assume a value of $\beta = 2.66$ eV for carbon π systems.[31] The Fermi level is then found at $E = 0$, and one-half of the levels are occupied.

The Hückel method is applicable with reasonable accuracy to planar systems where the states close to the Fermi level are governed by s (e.g., alkali metals or hydrogen), p_z (carbon), or d_{z^2} (transition metals) orbitals. In these systems, the interaction energy is governed by those orbitals that are normal to the plane that hosts the atomic skeleton of the system (see Figure 2). Hence, the Hückel method can be used for studying

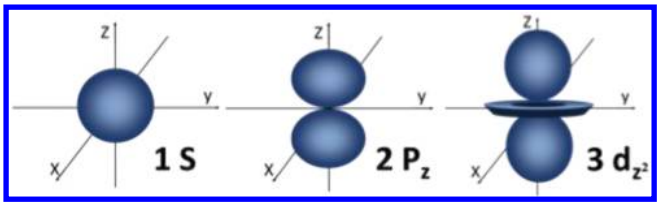

Figure 2. Graphical representation of 1s, $2p_z$, and $3d_{z^2}$ orbitals.

metallic transition metal dichalcogenide nanostructures, where the metallic character is determined by the d_{z^2} orbitals, and possibly for other systems. Thus, for NbS_2 and ReS_2, only one valence d_{z^2} orbital per transition metal atom is considered in the calculation and all other electrons, including those of the sulfur atoms, are neglected. The interatomic distance cutoff used to define bonds was set 3.4 Å, a value that is larger than the next neighbor but shorter than the second next neighbor distance. We should note, however, that our tool is restricted to the Γ-point approximation. Consequently, it cannot be used to determine the correct band gap (here, we speak of a band gap only if the band structure has been calculated for reasons seen later in this article) but instead for the gap at the Γ point, Δ_Γ, which is equivalent to the "HOMO–LUMO gap" $\epsilon_{n/2+1} - \epsilon_{n/2}$ within the "molecular interpretation". To assess the full electronic picture given by Hückel theory, reflected in the band structure, we created a Hückel-compatible Slater–Koster table[32] which can be used within the common DFTB implementations and is available in the Supporting Information.

dx.doi.org/10.1021/ct3003496 | J. Chem. Theory Comput. XXXX, XXX, XXX–XXX

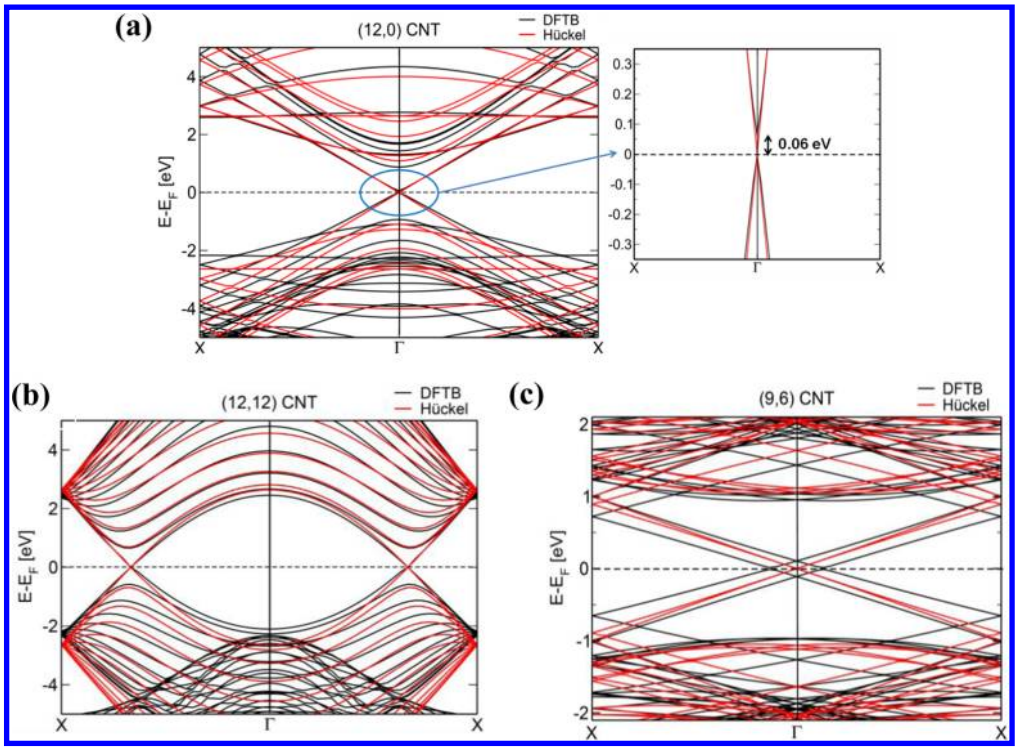

Figure 3. Band structures of (a) zigzag (12,0), (b) armchair (12,12), and (c) chiral (9,6) carbon nanotubes calculated using DFTB and Hückel methods. Horizontal dashed lines indicate the Fermi level.

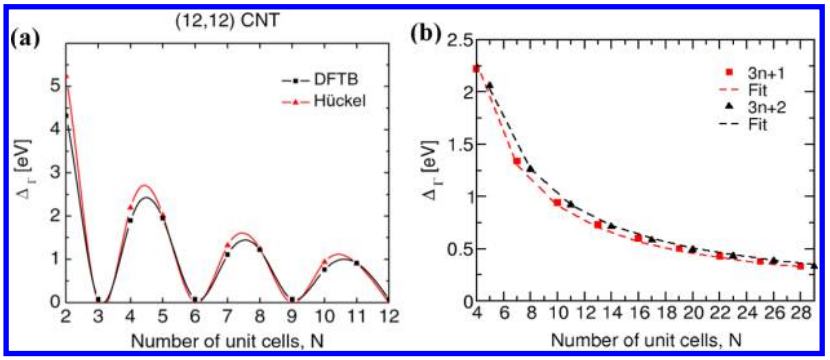

Figure 4. (a) Gap energies at the Γ point (Δ_Γ) versus number of primitive cells N in the simulation box for the (12,12) CNT. (b) Δ_Γ as function of C/N for two types of supercells: $N = 3n + 1$ and $3n + 2$ of the (12,12) CNT, n being an integer and C being a constant. C is 9.11 and 10.15 eV for supercells of the $3n + 1$ and $3n + 2$ type, respectively.

Periodic DFTB[14,16,33] calculations have been carried out within the DFTB+ code[28] for band structures, and for Γ-point supercell simulations the deMonNano[34] code has been used. Band structures have been calculated using high-symmetry k points in the Brillouin zone (BZ) along the paths X−Γ−X and Γ−M−K−Γ for nanotubes and monolayers, respectively. We further used 30 k points between high-symmetry points to obtain smooth curves.

The geometries of transition metal dichalcogenides have been reported earlier and are taken from refs 35 and 36. The carbon structures have been fully optimized using the DFTB method[14,16] within the Γ-point approximation as implemented in the deMonNano code.[34]

RESULTS AND DISCUSSION

1. Carbon Nanotubes. Carbon nanotubes are semiconducting unless the chiral indexes satisfy the relation $(n - m)/3 \in I$.[37] This implies that all armchair tubes and also zigzag tubes with a primary index being a multiple of 3 are metallic. The theoretical origin of the band folding has been discussed in detail earlier.[38,39] Figure 3 shows the band structure of three exemplary CNT. The Dirac point of a zigzag (12,0) CNT is located at the center of the reciprocal cell (Γ point) (see Figure 3a). Hence, with the same arguments as in ref 39, the supercell method folds the Dirac point to the Γ point for supercells containing $3N$ primitive cells, with N describing the number of primitive cells, and N being an integer.

Indeed, for the (12,12) armchair tube (see Figure 3b) the band crossing occurs at two-thirds between the Γ and X high-symmetry points. Therefore, the Γ-point approximation gives nonzero gap values at the Γ point (Δ_Γ) for supercells that contain a number of primitive cells N that are not multiples of 3 (cf. Figure 4a). (Hereafter, we will use Δ_Γ for gaps at the Γ point and Δ for band gaps obtained from band structure calculations. Note that Δ_Γ depends on N, the number of primitive cells in the supercell.) The Δ_Γ values for supercells

dx.doi.org/10.1021/ct3003496 | J. Chem. Theory Comput. XXXX, XXX, XXX−XXX

Table 1. Gap Energies at the Γ Point, Δ_Γ (in eV), of Carbon Nanotubes with Different Chiralities Calculated Using the DFTB and Hückel (H) Methods

chirality	(9,0)		(12,0)		(7,7)		(12,12)		(9,6)	
N	DFTB	H	DFTB	H	DFTB	H	DFTB	H	DFTB	H
2	0.102	0.00	0.06	0.00	4.16	5.41	4.32	5.41	0.23	0.00
3	0.102	0.00	0.06	0.00	0.26	0.00	0.08	0.00	0.23	0.00
4	0.102	0.00	0.06	0.00	1.79	2.24	1.90	2.24	0.23	0.00
5	0.102	0.00	0.06	0.00	2.18	2.06	1.95	2.06	0.23	0.00
6	0.102	0.00	0.06	0.00	0.26	0.00	0.08	0.00	0.23	0.00
7	0.102	0.00	0.06	0.00	0.97	1.34	1.11	1.34	0.23	0.00
8	0.102	0.00	0.06	0.00	1.44	1.26	1.22	1.26	0.23	0.00
9	0.102	0.00	0.06	0.00	0.26	0.00	0.08	0.00		
10	0.102	0.00	0.06	0.00	0.61	0.94	0.76	0.94		
11	0.102	0.00	0.06	0.00	1.11	0.92	0.91	0.92		
12	0.102	0.00	0.06	0.00	0.26	0.00	0.08	0.00		

with N not being a multiple of 3 converge very slowly as a function of C/N (with C being a constant) to small numbers (Figure 4b). Even for 30 primitive cells Δ_Γ takes values of ∼300 meV, and the metallic character of the system is not obvious from these calculations. A typical supercell containing 11 primitive cells and hence comprising 528 atoms still has an appreciable Δ_Γ of ∼1 eV (Figure 4a) and gives a good setup for Car−Parrinello (CP) simulations. For the chiral (9,6) tube, the symmetry break shifts the Dirac point off the high-symmetry points (see Figure 3c). Therefore, they will not be folded exactly to the Γ point, but the same general trend for Δ_Γ holds as for the armchair tubes.

The Hückel method gives excellent estimates of Δ_Γ compared to DFTB, which makes it a very useful tool for preprocessing very large structures due to its computational simplicity.Table 1 shows that for a variety of CNT chiralities Hückel theory estimates correctly $\Delta_\Gamma(N)$, and we generalize these findings for armchair CNTs. Figure 5 shows that the calculation using the Γ-point approximation significantly affects the density of states (DOS) for medium-sized supercells, as shown for the example of the (12,12) CNT. The DOS has a nonzero value at the Fermi energy for the nanotube contaning 3 primitive cells and zero value for N = 4 and 5. For larger supercells (N > 11), the electronic DOS converges to the expected result.

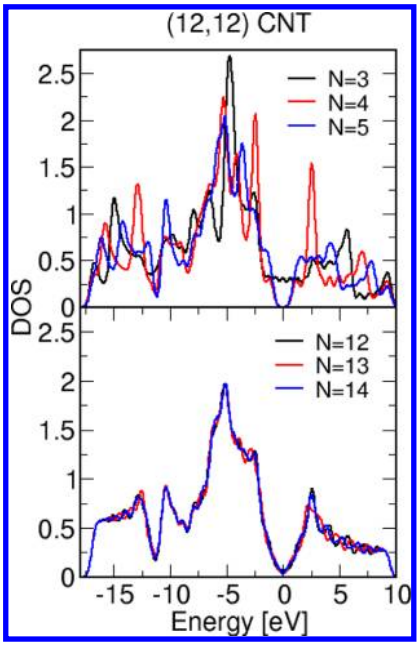

Figure 5. Density of states (DOS) of the (12,12) CNT calculated by broadening the one-particle energies obtained for the Γ point. N represents the number of unit cells.

Let us focus on the band structures of metallic zigzag CNTs, those with chirality (n,0), n being a multiple of 3. For the (12,0) CNT, Hückel theory predicts no band gap, while the DFTB model shows a small band gap of 60 meV (see Figure 3a), in agreement with DFT calculations reported in the literature.[40] The curvature of a carbon nanotube has an effect on the sp^2 hybridization and leads to small interactions between the π orbitals and the σ framework. Those cause a small band gap (on the order of some 10 meV) for nanotubes with small diameters.[40] Obviously, Hamiltonians describing only the π system, such as the tight-binding or Hückel models, fail to describe this effect. For smaller tubes, the gap opening further increases (to 0.1 eV in the case of the (9,0) tube, Table 1). In summary, Hückel theory and DFTB yield similar results for the energy bands around the Fermi level for large-diameter CNTs.

In order to evaluate if the Γ-point approximation is able to produce correct geometries, we optimized the tubes with and without k sampling and discuss here the (6,6) CNT as a prototype. After optimization of the supercell (N = 8, Γ-point approximation) and the primitive cell (30 k points), we computed the band structures of the resulting geometries (shown in Figure 6). Both geometries are in a very close agreement; in particular, the geometry obtained using the Γ-point approximation correctly yields the Dirac point between X and Γ. However, its slightly different symmetry gives rise to a very small shift of the bands, and a minor splitting is observed. The shift gets smaller with increasing size of the nanotube.

2. Graphene and Graphene Nanoribbons. The massive interest in the electronic properties of graphene and graphene nanoribbons (GNR) motivated us to explore the performace of the Γ-point approximation also for those systems.[41,42] For a single layer of graphene, periodic boundary conditions were employed in both directions (a and b) to a representative supercell (cf. Figure 1). Using a standard hexagonal unit cell, we found that the band gap oscillates and becomes zero only for supercells that are a multiple of three primitive cells. In the following, we will concentrate on supercells with rectangular shape. The initial supercell contains 6 and 10 unit cells along armchair (a) and zigzag (b) directions, respectively. (Hereafter, we will refere to number of unit cells in a and b directions as N_a

dx.doi.org/10.1021/ct3003496 | J. Chem. Theory Comput. XXXX, XXX, XXX−XXX

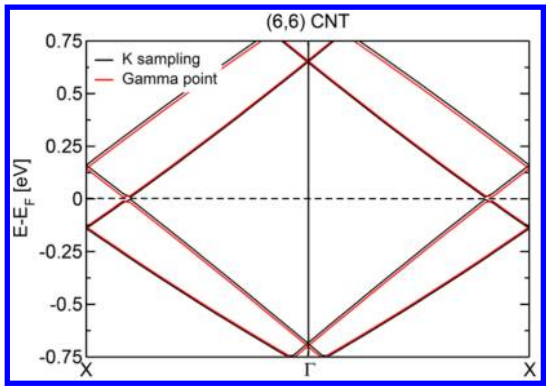

Figure 6. Band structures of the (6,6) CNT optimized within k sampling (black lines) and the Γ-point approximation (red lines) using a primitive cell and the supercell (8 unit cells), repsectivelly. Horizontal dashed lines indicate the Fermi level.

and N_b, respectively.) To capture the effect of zone folding at the Γ point, we calculated Δ_Γ (N_b) as we enlarged the graphene supercell in the b direction while N_a remained fixed, and then we varied N_a with fixed N_b. Indeed, extending the graphene supercell by adding unit cells along the b direction leads to variation in Δ_Γ. As indicated in Figure 7a (values are given in Table 2), the dependence of Δ_Γ on the number of cells along the zigzag direction (N_b) gives a very similar trend as the results for the nanotubes shown in Figure 4, while no change is observed upon modification of the number of primitive cells along armchair direction (N_a). The band structure of graphene along the high-symmetry Γ−M−K−Γ path is presented in Figure 7b. The DFTB and Hückel models yield comparable results for the wave vectors close to the K point, where the valence and conduction bands cross each other at the Fermi level. However, in DFTB the bands responsible for the σ framework are located at higher energy than π, particularly around the Γ point. As a result, the Hückel Hamiltonian at the Γ point does not reflect the gap correctly.

Graphene nanoribbons (GNRs) have been constructed by cutting a graphene sheet with the selected edge topology (zigzag or armchair) and GNR widths (N_w) (see Figure 8). N_w has a physical meaning, and it denotes the finite size of a GNR in the graphene plane. Again, we studied the influence of the size of the supercell (N) and also N_w on the band gaps. The quasi-1D nature of GNRs leads to confinement effects for the π electrons. For DFTB calculations, each carbon atom at edges of the GNRs is terminated by one hydrogen atom in order to remove spurious radicaloid states close to the Fermi level. All GNR structures were fully optimized regarding atomic positions and lattice constant. Both parameters N_w and N were varied in such a way that for a given N_w (3−10) we studied various supercell sizes, N (1−10). One-dimensional periodic boundary conditions were applied along the ribbon axis.

The resulting exemplary band structures of two armchair and two zigzag GNRs are shown in Figure 9. N_w leads to emerging confined electronic states close to the Dirac point for ribbons with armchair edges. As a result, the electronic structure of armchair GNRs depends strongly on N_w (see Figure 9a and 9b), while in zigzag GNRs it is independent of the ribbon width and the gap is always zero (see Figure 9c and 9d).

For the armchair GNRs the Dirac point is always folded into the Γ point. Therefore, Δ_Γ is independent of N, counting the number of primitive cells in the quasi-1D periodic structure of the ribbons. More importantly, the GNRs always have a direct band gap at the Γ point, and $\Delta_\Gamma = \Delta$. In the case of zigzag GNRs, as shown in Figure 9c and 9d, the band structure is always characterized by a band of very small dispersion around the Γ point and the ribbons are found to be metallic independent of N, well characterized by Δ_Γ. Earlier experimental and theoretical studies reported that the band gap is inversely proportional to the width of the graphene nanoribbons.[43,44] However, the band gap of armchair GNRs oscillates with increasing width (N_w) of the ribbons (Figure 10a). Although Δ_Γ oscillates, it also decreases with increasing N_w and is expected to reach zero for very wide GNRs that would closely resemble the structure of graphene. At the same time, the band gap of zigzag GNRs is zero and remains constant with various sizes of N_w. The explanation for this behavior can be described by discussing the allowed $\boldsymbol{k}$ vectors projected into the Brillouin zone of graphene: Due to the edge-induced boundary condition, the wavevectors are quantized along the ribbon width (see Figure 10b for an illustration for two types of GNR). The allowed wavevectors are separated by $\Delta K_\perp = ((2\pi)/(((2N_w-1)a))$ and $\Delta K_\perp = ((2\pi)/(\sqrt{3}(2N_w-1)a))$ for armchair and zigzag GNRs, respectively (where a is the lattice constant of graphene). Our results demonstrate that armchair nanoribbons with $N_w = 3M + 1$ ($M \in I$) are metallic, while for all the other cases the allowed lines do not pass through the point K, and therefore, armchair nanoribbons are semiconducting (see Table 3), as reported elsewhere.[45] In the case of zigzag GNRs, the confined states do not emerge from the same Dirac point but from two independent points, $\boldsymbol{K}$ and $\boldsymbol{K}'$, which results in the metallic character of the electronic structure (cf. Figure 10b).

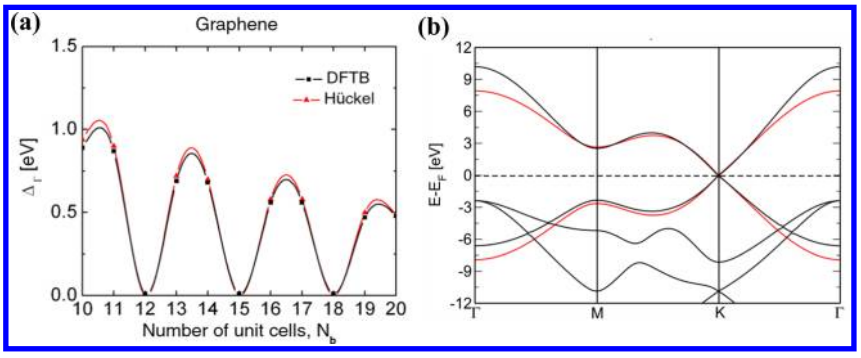

Figure 7. (a) Energy gaps at the Γ point, Δ_Γ, versus number of primitive cells in zigzag direction N_b in the simulation box, and (b) band structure of graphene. Solid black and red lines correspond to the DFTB and Hückel methods, respectively.

dx.doi.org/10.1021/ct3003496 | J. Chem. Theory Comput. XXXX, XXX, XXX−XXX

Table 2. Energy Gaps at the Γ Point (Δ_Γ in eV) of Graphene Calculated Using the DFTB and Hückel Methods[a]

N_b	10	11	12	13	14	15	16	17	18	19	20
DFTB	0.89	0.87	0.01	0.69	0.68	0.01	0.56	0.56	0.01	0.47	0.48
H	0.94	0.92	0.00	0.74	0.72	0.00	0.60	0.58	0.00	0.50	0.50

[a]Note that changing the N_a of graphene supercell does not influence the gap energies for a given N_b.

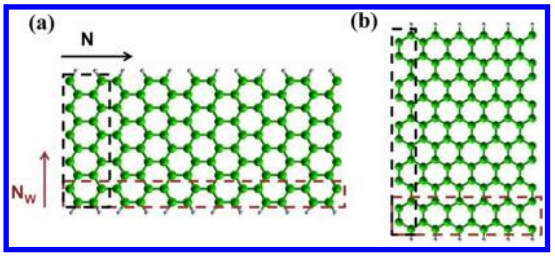

Figure 8. Atomistic scheme of the (a) armchair and (b) zigzag GNR N_w = 5 and N = 6 unit cells. Dashed rectangles indicate the unit cells in the armchair and zigzag directions of the ribbons.

3. Transition Metal Dichalcogenides. In addition to graphene and carbon nanotubes, many other layered materials exist in nature, and it has been shown that they are able to form monolayers and nanotubes.[46,47] The systems are, depending on the stoichiometry, metallic, semiconducting, or insulating. We focus here on transition metal dichalcogenides, as this family has recently proven to be particularly interesting as the first transistor,[48] and the first integrated circuits[49] fabricated using MoS_2 monolayers have been reported by Kis and co-workers. Transition metal dichalcogenides TX_2 (T = Mo, Nb, W, Re, Ti; X = S, Se, Te) are an intriguing family of inorganic materials with potential to serve in nanoelectronic applications. They can be metallic or semiconducting depending on their chemical composition and how their atoms are arranged.[50,51] While bulk MoX_2 or WX_2 are indirect band gap semiconductors, transforming to exhibit direct band gaps as monolayers, NbX_2 and ReX_2 are metals.[35] The TX_2 structures contain a metal layer sandwiched between two chalcogenide layers, with the metal in

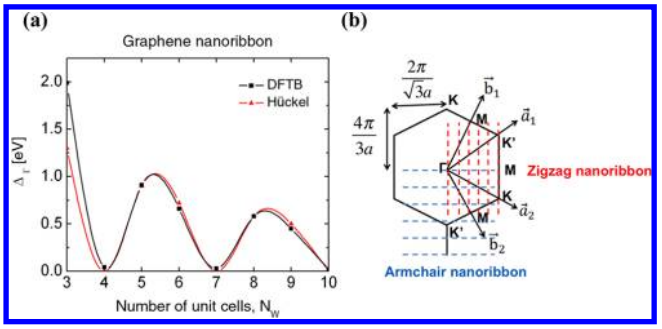

Figure 10. (a) Gap energies Δ_Γ versus N_w (number of unit cells defining the ribbon width) in the simulation box for armchair GNRs. (b) First hexagonal Brillouin zone of graphene. a_1 (a_2) and b_1 (b_2) indicate the lattice vectors and the reciprocal lattice vectors of graphene, respectively. Allowed wave vectors are indicated by dashed lines for armchair and zigzag GNRs with N_w = 3.

Table 3. Gap Energies Δ_Γ (in eV) of Armchair GNRs Calculated Using DFTB and Hückel Methods[a]

N_w	3	4	5	6	7	8	9	10
DFTB	1.99	0.04	0.91	0.66	0.03	0.58	0.45	0.02
H	1.35	0.00	0.91	0.73	0.00	0.58	0.49	0.00

[a]Note that changing the size of the GNR suercell N does not influence the gap energies for a given N_w.

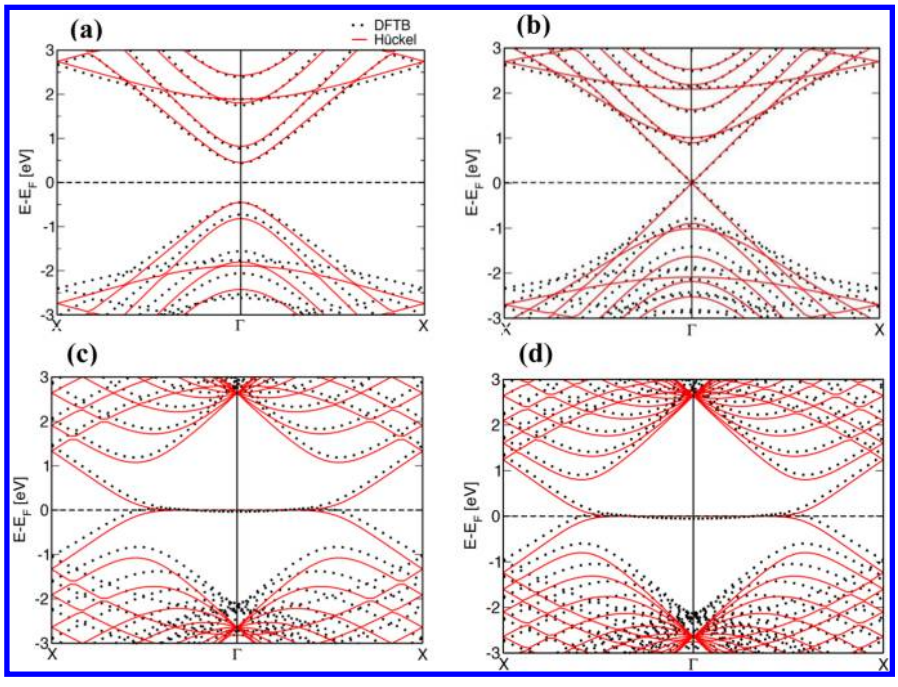

Figure 9. Band structures of (a, b) armchair GNRs and (c, d) zigzag GNRs. Energy bands have been calculated using DFTB and Hückel methods. Horizontal dashed lines indicate the Fermi level.

dx.doi.org/10.1021/ct3003496 | J. Chem. Theory Comput. XXXX, XXX, XXX−XXX

trigonal pyramidal or octahedral coordination. The layers of (X−T−X) are covalently bound, but additional metal bonds are present in the central layer formed by the transition metals T. Tubular structures can be analogously constructed by rolling up the sheets along specific directions in the 2D lattice.[52] The electronic band structures of NbS_2 and ReS_2 monolayers along the high-symmetry points using the path Γ−*M*−*K*−Γ are shown in Figure 11.

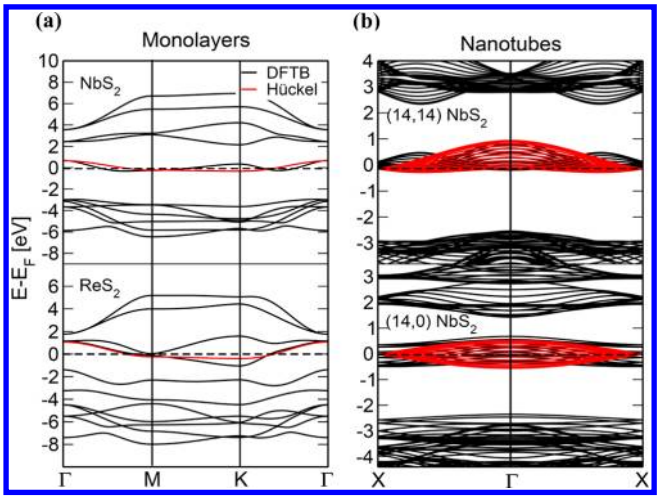

Figure 11. Band structures of (a) NbS_2 and ReS_2 monolayers and (b) NbS_2 armchair and zigzag nanotubes calculated using DFTB and Hückel methods. Horizontal dashed lines indicate the Fermi level.

The NbS_2 monolayer shows metallic behavior, which is caused by the Nb d band that crosses the Fermi level at several points within the Brillouin zone (Figure 11a). The results are in good agreement with DFT band structures of NbS_2 monolayer reported recently.[35] Deeper analysis reveals that the metallic character of NbS_2 and of other similar structures of this family, such as ReS_2, arises from half-filled d_{z^2} orbitals.[4] Therefore, as in carbon π systems, a single-band Hückel model, incorporating only the d_{z^2} orbitals of the transition metals and neglecting all remaining electrons of the transition metal and of the sulfur atoms, can be employed. Within the Hückel model, the electronic structure of the d_{z^2} bands near the Fermi level can be described with one parameter, $\beta = 0.15$ eV, that is the hopping matrix element. Figure 11a shows that the Hückel model reproduces well the band that crosses the Fermi level for the NbS_2 monolayer. Similarly, ReS_2 has one unpaired electron per metal atom and metallic character. The band located at the Fermi level arises from the 5d orbitals of Re atoms, and again, this band calculated at the Hückel level resembles nicely the one from DFTB calculations.

Similar as for CNTs, also for inorganic nanotubes the simple Hückel model cannot account for effects due to the curvature of the tubes. Therefore, differences to all-valence-electron band structure calculations are expected (Figure 11b). Nonetheless, as this simple model allows a great reduction of complexity as might be used for model considerations in order to understand electronic processes in these systems and might be applied to other metallic materials of this family, including doped semiconducting TX_2 layers and nanotubes.

Figure 12 shows the density of states (DOS) calculated within the Γ-point approximation for NbS_2 nanotubes with different number of primitive cells *N* in the supercell. Contrary

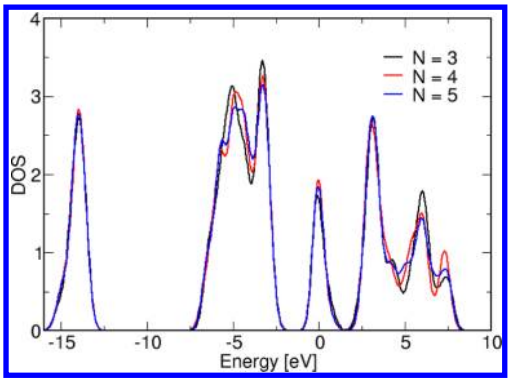

Figure 12. Density of states (DOS) for the (14,14) NbS_2 nanotube calculated using the Γ-point approximation and DFTB method. *N* indicates the number of unit cells in the supercell.

to CNT, the DOS converges quickly with respect to the number of primitive cells (*N*) in the supercell approach.

Both Hückel and DFTB calculations demonstrate that Δ_Γ is independent of the size of supercell *N* and remains zero for all NbS_2 and ReS_2 nanotubes, as well as for their corresponding monolayers.

CONCLUSION

We indicated that the Γ-point approximation can be employed for supercell simulations of carbon nanotubes, graphene and graphene nanoribbons, inorganic nanotubes, and inorganic 2D materials if the simulation box is chosen carefully. We have shown that it is possible to choose simulation boxes that have a reasonable energy gap at the Γ point that allows efficient calculations using the Car−Parrinello method. Alternatively, for the same systems, the supercells can be chosen in a way that the metallic character of the system is reflected at the Γ point.

To allow an educated estimation of the electronic structure of those systems at the Γ point, we developed a simple Hückel code that is available as Supporting Information.

Finally, we evaluated the tight-binding (Hückel) model for transition metal dichalcogenide layers and nanotubes and conclude that it provides a simple and affordable approach to estimate their electronic structures close to the Fermi level.

We want to point out that the validity and limits of those simple one-electron models, often employed for fundamental considerations in physics, can be tested conveniently using the Hückel code provided with this article, and it can be directly compared to more sophisticated models, as, for example, the DFTB method.

ASSOCIATED CONTENT

Supporting Information

Manual of the Hückel code, examplary test calculations, and Slako files created for Hückel method. This material is available free of charge via the Internet at http://pubs.acs.org. Source code can be obtained free of charge at http://ses.jacobs university.de/ses/theine/research.

AUTHOR INFORMATION

Corresponding Author

*E-mail: t.heine@jacobs-university.de.

Notes

The authors declare no competing financial interest.

dx.doi.org/10.1021/ct3003496 | *J. Chem. Theory Comput.* XXXX, XXX, XXX−XXX

■ ACKNOWLEDGMENTS

This work was supported by FP7-PEOPLE-ITN-2008 "NanoCTM" (GA 234970), REA-FP7-MC-IAPP "QUASINANO" (GA 251149), and the German Research Council (DFG, grant HE 3543/18-1). We thank Dr. Stefano Borini (SCM NV, Amsterdam, The Netherlands) for support in writing the Hückel code. Carbon nanotube structures were generated using GTK Display Interface for Structures GDIS 0.90.

■ REFERENCES

(1) Saito, R.; Dresselhaus, G.; Dresselhaus, M. S. Electronic Structure of Single-Wall Nanotubes. *Physical properties of carbon nanotubes*; Imperial College Press: London, 1998.
(2) Geim, A. K.; Novoselov, K. S. *Nat. Mater.* **2007**, *6*, 183.
(3) Guimaraes, L.; Enyashin, A. N.; Frenzel, J.; Heine, T.; Duarte, H. A.; Seifert, G. *ACS Nano* **2007**, *1*, 362.
(4) Ivanovskaya, V. V.; Enyashin, A. N.; Medvedeva, N. I.; Ivanovskii, A. L. *Phys. Status Solidi B* **2003**, *238*, R1−R4.
(5) Ivanovskaya, V. V.; Heine, T.; Gemming, S.; Seifert, G. *Phys. Status Solidi B* **2006**, *243*, 1757.
(6) Kaplan-Ashiri, I.; Cohen, S. R.; Gartsman, K.; Ivanovskaya, V.; Heine, T.; Seifert, G.; Wiesel, I.; Wagner, H. D.; Tenne, R. *Proc. Natl. Acad. Sci. U.S.A.* **2006**, *103*, 523.
(7) Kaplan-Ashiri, I.; Cohen, S. R.; Gartsman, K.; Rosentsveig, R.; Ivanovskaya, V.; Heine, T.; Seifert, G.; Wagner, H. D.; Tenne, R. *Mater. Sci. Forum* **2005**, *475*, 4097.
(8) Kuc, A.; Enyashin, A.; Seifert, G. *J. Phys. Chem. B* **2007**, *111*, 8179.
(9) Kuc, A.; Heine, T. *Adv. Mater.* **2009**, *21*, 4353.
(10) Seifert, G.; Terrones, H.; Terrones, M.; Jungnickel, G.; Frauenheim, T. *Phys. Rev. Lett.* **2000**, *85*, 146.
(11) Teich, D.; Lorenz, T.; Joswig, J.-O.; Seifert, G.; Zhang, D.-B.; Dumitrica, T. *J. Phys. Chem. C* **2011**, *115*, 6392.
(12) Elstner, M. *Theor. Chem. Acc.* **2006**, *116*, 316.
(13) Frauenheim, T.; Seifert, G.; Elstner, M.; Hajnal, Z.; Jungnickel, G.; Porezag, D.; Suhai, S.; Scholz, R. *Phys. Status Solidi B* **2000**, *217*, 41.
(14) Seifert, G.; Porezag, D.; Frauenheim, T. *Int. J. Quantum Chem.* **1996**, *58*, 185.
(15) Elstner, M.; Porezag, D.; Jungnickel, G.; Elsner, J.; Haugk, M.; Frauenheim, T.; Suhai, S.; Seifert, G. *Phys. Rev. B* **1998**, *58*, 7260.
(16) Oliveira, A. F.; Seifert, G.; Heine, T.; Duarte, H. A. *J. Braz. Chem. Soc.* **2009**, *20*, 1193.
(17) Astala, R.; Kaukonen, M.; Nieminen, R. M.; Heine, T. *Phys. Rev. B* **2000**, *61*, 2973.
(18) Haugk, M.; Elsner, J.; Heine, T.; Frauenheim, T.; Seifert, G. *Comput. Mater. Sci.* **1999**, *13*, 239.
(19) Sternberg, M.; Frauenheim, T.; Zimmermann-Edling, W.; Busmann, H.-G. *Surf. Sci.* **1997**, *370*, 232.
(20) Di Carlo, A.; Gheorghe, M.; Bolognesi, A.; Lugli, P.; Sternberg, M.; Seifert, G.; Frauenheim, T. *J. Comput. Electron* **2002**, *1*, 109.
(21) Seifert, G.; Kaschner, R.; Schone, M.; Pastore, G. *J. Phys.: Condens. Matter* **1998**, *10*, 1175.
(22) Heine, T.; Seifert, G.; Fowler, P. W.; Zerbetto, F. *J. Phys. Chem. A* **1999**, *103*, 8738.
(23) Ahlswede, B.; Jug, K. *J. Comput. Chem.* **1999**, *20*, 563.
(24) Parrinello, M.; Hutter, J.; Marx, D.; Focher, P.; Tuckerman, M.; Andreoni, W.; Curioni, A.; Fois, E.; Roetlisberger, U.; Giannozzi, P.; Deutsch, T.; Alavi, A.; Sebastiani, D.; Laio, A.; VandeVondele, J.; Seitsonen, A.; Billeter, S. *CPMD*; Copyright IBM Corp. and MPI-FKF: Stuttgart, 1995.
(25) Blöchl, P. E. *Phys. Rev. B* **1994**, *50*, 17953.
(26) Soler, J. M.; Artacho, E.; Gale, J. D.; García, A.; Junquera, J.; Ordejón, P.; Sánchez-Portal, D. *J. Phys.: Condens. Matter* **2002**, *14*, 2745. VandeVondele, J.; Krack, M.; Mohamed, F.; Parrinello, M.; Chassaing, T.; Hutter J., *Comput. Phys. Commun.* **2005**, *167*, 103. For more information, please look at CP2K code: http://www.cp2k.org/.
(27) Burdett, K. J. *Prog. Solid State Chem.* **1984**, *15*, 173.
(28) Aradi, B.; Hourahine, B.; Frauenheim, T. *J. Phys. Chem. A* **2007**, *111*, 5678.
(29) Wang, S.; Grifoni, M. *Phys. Rev. Lett.* **2005**, *95*, 266802.
(30) Negri, F.; Orlandi, G.; Zerbetto, F. *J. Am. Chem. Soc.* **1991**, *113*, 6037.
(31) Mintmire, J. W.; White, C. T. *Carbon* **1995**, *33*, 893.
(32) Slater, J. C.; Koster, G. F. *Phys. Rev.* **1954**, *94*, 1498.
(33) Porezag, D.; Frauenheim, T.; Kohler, T.; Seifert, G.; Kaschner, R. *Phys. Rev. B* **1995**, *51*, 12947.
(34) Heine, T.; Rapacioli, M.; Patchkovskii, S.; Frenzel, J.; Koester, A. M.; Calaminici, P.; Escalante, S.; Duarte, H. A.; Flores, R.; Geudtner, G.; Goursot, A.; Reveles, J. U.; Vela, A.; Salahub, D. R. *deMon-nano*; Jacobs University: Bremen, 2009.
(35) Kuc, A.; Zibouche, N.; Heine, T. *Phys. Rev. B* **2011**, *83*, 245213.
(36) Zibouche, N.; Kuc, A.; Heine, T. *Eur. Phys. B* **2012**, *85*, 49.
(37) Wilder, J. W. G.; Venema, L. C.; Rinzler, A. G.; Smalley, R. E.; Dekker, C. *Nature* **1998**, *391*, 59.
(38) Hamada, N.; Sawada, S.-ichi; Oshiyama, A. *Phys. Rev. Lett.* **1992**, *68*, 1579.
(39) Li, T. L. *Electronic Structures of Single-Wall Carbon Nanotubes*; National Chia-Yi University, Department of Applied Physics: Chiayi, Taiwan, Republic of China, 2009.
(40) Blase, X.; Benedict, L. X.; Shirley, E. L.; Louie, S. G. *Phys. Rev. Lett.* **1994**, *72*, 1878.
(41) Saffarzadeh, A.; Ghorbani Asl, M. *Eur. Phys. J. B* **2009**, *67*, 239.
(42) Kuc, A.; Heine, T.; Seifert, G. *Phys. Rev. B* **2010**, *81*, 85430.
(43) Han, M. Y.; Ozyilmaz, B.; Zhang, Y.; Kim, P. *Phys. Rev. Lett.* **2007**, *98*, 206805.
(44) Son, W.-Y.; Cohen, M. L.; Louie, S. G. *Phys. Rev. Lett.* **2006**, *97*, 216803.
(45) Palacios, J. J.; Fernández-Rossier, J.; Brey, L.; Fertig, H. A. *Semicond. Sci. Technol.* **2010**, *25*, 033003.
(46) Tenne, R.; Remškar, M.; Enyashin, A.; Seifert, G. Inorganic Nanotubes and Fullerene-Like Structures (IF). *Topics in Applied Physics, Carbon Nanotubes*; Springer: Berlin/Heidelberg, 2008; Vol. *111*, p 631.
(47) Tenne, R.; Margulis, L.; Genut, M.; Hodes, G. *Nature* **1992**, *360*, 444.
(48) Radisavljevic, B.; Radenovic, A.; Brivio, j; Giacometti, V.; Kis, A. *Nat. Nanotechol.* **2011**, *6*, 147.
(49) Bertolazzi, S.; Brivio, J.; Kis, A. *ACS Nano* **2011**, *5*, 9703.
(50) Wilson, J. A.; Yoffe, A. D. *Adv. Phys.* **1969**, *18*, 193.
(51) Marseglia, E. A. *Int. Rev. Phys. Chem.* **1983**, *3*, 177.
(52) Seifert, G.; Köhler, T.; Tenne, R. *J. Phys. Chem. B* **2002**, *106*, 2497.